# How Surface Stress Transforms Surface Profiles and Adhesion of Rough Elastic Bodies

Chung-Yuen Hui[1,2*], Zezhou Liu[1], Nicolas Bain[3], Anand Jagota[4], Eric R. Dufresne[3], Robert W. Style[3], Ryuji Kiyama[5] and Jian Ping Gong[2,6,7]

[1]Field of Theoretical and Applied Mechanics, Sibley School of Mechanical and Aerospace Engineering, Cornell University, Ithaca, NY 14853, USA

[2] Global Station for Soft Matter, GI-CoRE, Hokkaido University, Sapporo, Japan

[3]Laboratory of Soft and Living Materials, Department of Materials, ETH Zürich, 8093 Zürich, Switzerland

[4]Departments of Bioengineering and of Chemical & Biomolecular Engineering, 111 Research Drive, Lehigh University, Bethlehem, PA 18015, USA

[5]Graduate School of Life Science, Hokkaido University, Sapporo 001-0021, Japan.

[6]Faculty of Advanced Life Science, Hokkaido University, Sapporo 001-0021, Japan.

[7]WPI-ICReDD, Hokkaido University, Sapporo 001-0021, Japan.

[*]Corresponding Author, 322 Thurston Hall, Cornell University, Ithaca, NY 14853, USA. ch45@cornell.edu

**Abstract:** The surface of soft solids carries a surface stress that tends to flatten surface profiles. For example, surface features on a soft solid, fabricated by molding against a stiff patterned substrate, tend to flatten upon removal from the mold. In this work we derive a transfer function in explicit form that, given any initial surface profile, shows how to compute the shape of the corresponding flattened profile. We provide analytical results for several applications including flattening of 1D and 2D periodic structures, qualitative changes to the surface roughness spectrum, and how that strongly influences adhesion.

**Keywords:** surface stress; transfer function; flattening; surface roughness spectrum; adhesion

## 1. Introduction

Over the past decade, numerous studies have established that the surface stress $\sigma$ of soft solids plays an important and often dominant role in a variety of mechanical and physical phenomena [1]. In simple liquids, surface energy and the corresponding isotropic and constant surface stress, are numerically identical and surface stress is referred to as surface tension. In this work we assume that the solid surface stress is likewise constant and isotropic and in this way the surface is fluid-like. For bulk elastic materials, the effects of surface stress are typically felt over a characteristic elastocapillary length, $l_c \sim \beta\sigma / 2G$, where $G$ is the shear modulus of the soft solid and constant $\beta = 2(1-\nu)$ is introduced for later convenience ($\nu$ is Poisson's ratio). Often, surface stress

is isotropic and approximately constant (per unit deformed area). Its value lies in a relatively narrow range, 10 – 100 mN/m for soft solids such as elastomers and gels and up to a few N/m for metals and ceramics [2–4]. However, for the same range of materials, elastic modulus varies over seven orders of magnitude. For metals, ceramics and some stiff silicones like PDMS, the value of elastocapillary length is generally very small [1,5]. For soft solids such as elastomers and gels with elastic modulus in the kPa to MPa range, the corresponding value of elastocapillary length is on the order of tens of nanometers to hundreds of microns or larger. Thus, for soft materials, surface stress is far more likely to play a significant and sometimes dominant role in surface mechanical phenomena.

For example, the surface stress can drive Rayleigh-Plateau-like instabilities [6]; it rounds off sharp edges by deformation [7–9]; it alters the flow field in porous media [10,11]. The contact mechanics models of Hertz and Johnson-Kendall-Roberts (JKR), which have been widely used to interpret indentation experiments, may no longer be applicable [12–17]. The contact angle of a liquid drop on a compliant surface is not a material property – it cannot be predicted by Young's equation – but depends on the surface stress of the solid substrate as well as its elasticity [18–29]. The modulus of many biological cells is on the order of kPa, and the behavior of such cells on hydrophobic surfaces is strongly influenced by surface stress [30]. If the characteristic length scale in a problem is $L$, say the diameter of a droplet, then one may define an elastocapillary number as the ratio of the elastocapillary length and $L$: $\sim l_c / L$ . Elastocapillary effects are generally important when the elastocapillary number approaches and exceeds unity in value. The flattening due to surface stress of a patterned surface bounding an elastic body is one of the basic phenomena that illustrates the action of surface stress. It has been used successfully to measure surface stress, and its dependence on strain [31–33]. Previous experimental work and accompanying analyses have focused on flattening of simple one-dimensional periodic surface patterns. Here we consider the problem of flattening due to surface stress of a general surface bounding an elastic body. In Section 2, we present a simple but general result (transfer function) that directly shows how to obtain the flattened shape in terms of the shape of the surface absent any surface stress. In Section 3.1 we apply this result to study how several 2D surfaces transform under the influence of surface stress. For periodic surfaces in 2D we show that in the limit of large elastocapillary number (based on largest wavelength) the transformed surface has a shape that is independent of the elastocapillary number. We additionally present results for shape change of an isolated bump or cavity.

In section 3.2 we consider the surface-stress driven transformation of rough surfaces. The role of roughness in a variety of surface mechanical phenomena is well-known [34–37]. In particular, surface roughness accounts for the discrepancy, for stiff bodies, between strong adhesion at the microscopic scale and lack of it at the macroscopic scale.[35,38]. Early models represented surface roughness by spherical asperities, and derived results by application of continuum contact mechanics [39,40]. However, most rough surfaces are random and

self-affine over a broad (nm – mm) range [36,37]. More recent work by Persson and others has revealed limitations of the spherical asperity approach and significant progress has been made on a mean-field theory based on the spectral properties of the roughness [41]. This approach has also been used to study adhesion between rough surfaces [42,43]. A key idea is that the energy required to bring rough surfaces into contact is released during their subsequent separation and is therefore subtracted from the intrinsic work of adhesion, lowering its value. It should be noted that Persson's approach does not apply to several specially designed surfaces where effects such as crack-trapping and local mechanical instabilities can lead to strong enhancement of adhesion with increasing roughness [44–46].

## 2. Flattening of a Surface: Relation Between Original and Flattened Profiles

We begin by posing the question: what is the relationship between the (initial) surface profile of an elastic body and the profile to which it transforms under the action of surface stress? We present simple transfer functions for 1D and 2D surfaces that convert the initial into its transformed shape. Fig. 1 depicts our system that comprises a soft elastic substrate, one face of which (with normal along $x_3$) is a macroscopically flat surface exposed to a liquid or gaseous phase. Microscopically, the profile of this surface can be randomly rough or patterned with some regular structure. The elastic substrate or body is very large in all its dimensions compared to length scales that characterize surface undulations; it is modeled as a half space with $x_3 > 0$ (Fig. 1). Denote the shear modulus and Poisson's ratio of the substrate by $G$ and $\nu$, respectively. Consider first a general 2D surface for which the initial surface profile (in the absence of surface stress) is defined by the function $h_0(x_1, x_2)$ with respect to $x_3 = 0$. For example, if the surface profile were fabricated by molding against a stiff patterned substrate, $h_0(x_1, x_2)$ would correspond to the surface pattern of the soft solid prior to its separation from the mold, i.e., the complement of the surface pattern of the mold itself. We denote by $h(x_1, x_2)$ the profile of the same surface under the action of surface stress. Then, the vertical surface displacement $u_3(x_1, x_2)$ is,

$$u_3 = h(x_1, x_2) - h_0(x_1, x_2). \tag{1}$$

Note, $h$ and $u_3$ are positive in the positive $x_3$ direction.

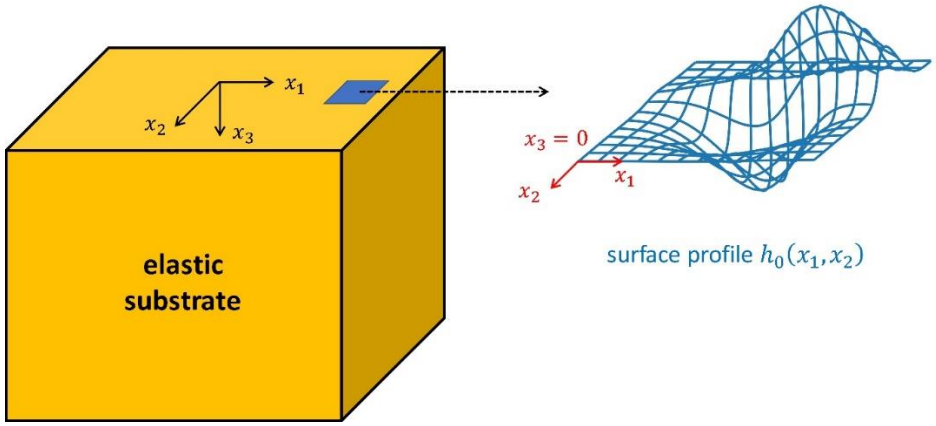


Fig. 1. Our system consists of an elastic substrate that is very large in all its dimensions compared to length scales that characterize surface undulations or structure.

Assume that the surface patterns are shallow and that the deformations are small. This allows two simplifications. Firstly, the surface profile can be used to compute the Laplace pressure acting on the deformed surface as

$$p_L\left(x_1, x_2\right) = \sigma \Delta h\,, \tag{2}$$

where $\Delta = \frac{\partial^2}{\partial x_1^2} + \frac{\partial^2}{\partial x_2^2}$ is the 2D Laplacian. Note that the pressure is calculated using the deformed (not the initial) shape, and that the surface stress is constant in the deformed shape. Here we use the standard notation that *compressive* pressure has a positive value. To calculate the response of the elastic solid to the Laplace pressure (Eq. (2)), we represent the body as a linearly elastic half-space bounded by a flat plane. In particular, we obtain the resulting vertical surface displacement $u_3$ as detailed in the supporting information (SI). Denoting the 2D Fourier transform (FT) operator by $F$, the FT of $h(\mathbf{x})$, $\tilde{h}(\mathbf{q})$, is

$$\tilde{h}(\mathbf{q}) = F\left[h(\mathbf{x})\right] \equiv \iint_D e^{-i(\mathbf{q}\cdot\mathbf{x})} h\left(x_1, x_2\right) dx_1 dx_2\,, \tag{3}$$

where $q_1$, $q_2$ are the transformed variables, $\mathbf{q} = \left(q_1, q_2\right)$ is the wave vector, $\mathbf{x} = \left(x_1, x_2\right)$, and $D$ is the physical domain. The inverse FT operator is denoted by $F^{-1}$

We now state the following elasticity result which is derived in the SI: the 2D FT of $u_3$, $\tilde{u}_3(\mathbf{q})$, is related to $\tilde{h}(\mathbf{q})$ by

$$\tilde{u}_3(\mathbf{q}) = -\frac{\beta\sigma}{2G} q\,\tilde{h}(\mathbf{q}), \tag{4}$$

where $\beta = 2(1-\nu)$ and $q = |\mathbf{q}| = \sqrt{q_1^2 + q_2^2}$ . The factor $\beta\sigma / 2G$ , with units of length, has previously been introduced as the elastocapillary length. It is important to note that $\beta = 2(1-\nu) \geq 1$. It equals unity for the special case of an incompressible solid, such as an elastomer. We also define the elastocapillary wave number (inverse elastocapillary length $l_c$) as

$$q_c \equiv 2G / \beta\sigma = 1 / l_c . \tag{5}$$

Taking the Fourier transform of (1) and using (4), we obtain a one-to-one relation between the Fourier transforms of the deformed and initial surfaces:

$$\tilde{h}(\mathbf{q}) = \tilde{h}_0(\mathbf{q}) / (1 + q / q_c). \tag{6}$$

Using standard terminology in control theory,

$$\tilde{\phi}(\mathbf{q}) \equiv [1 + q / q_c]^{-1}, \tag{7}$$

is the 2D transfer function. Because Fourier transforms of the profiles $h_0$, and $h$ are related multiplicatively through the transfer function in Fourier space, in physical space they are related through a convolution, i.e.,

$$h(x_1, x_2) = \iint_D \phi(x_1 - x_1', x_2 - x_2')\, h_0(x_1', x_2')\, dx_1' dx_2' , \tag{8a}$$

where $\phi(\mathbf{x})$ is the inverse Fourier transform of the transfer function, $\tilde{\phi}(\mathbf{q})$, which is (see the SI)

$$\phi(\mathbf{x}) = \frac{q_c^2}{2\pi}\left[\frac{1}{\bar{x}} - \frac{\pi}{2}\left[H_0(\bar{x}) - Y_0(\bar{x})\right]\right], \; \bar{x} \equiv q_c\sqrt{x_1^2 + x_2^2} \tag{8b}$$

where $H_0(\bar{x})$ is the Struve function of order zero, $Y_0(\bar{x})$ is the Bessel function of the second kind of order zero. A plot of the normalized transfer function $\bar{\phi} = 2\pi\phi / q_c^2$ versus $\bar{x}$ is shown in Fig. 2(a). For small and large $\bar{x}$ ,

$$\bar{\phi}(\bar{x} << 1) \approx \bar{x}^{-1} + \ln \bar{x} , \; \bar{\phi}(\bar{x} >> 1) \approx \bar{x}^{-3} \tag{8c,d}$$

The transfer function in Fourier space is also plotted in Fig. 2(b).

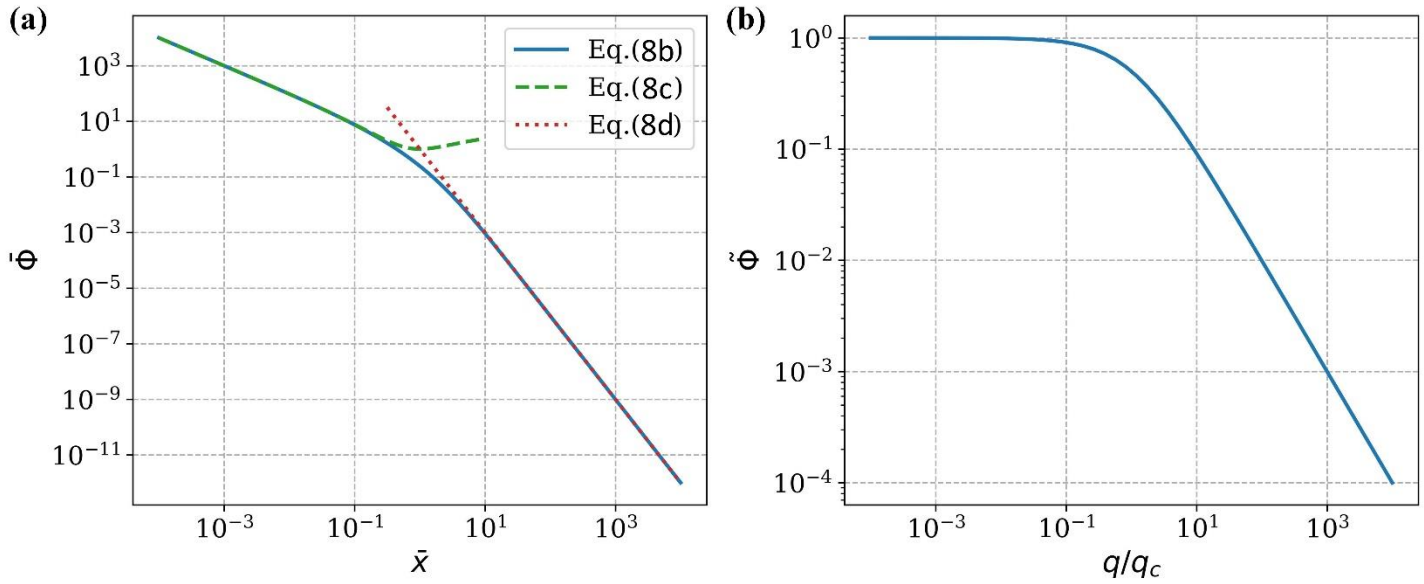


Fig. 2. (a) Normalized transfer function $\bar{\phi} = 2\pi\phi / q_c^2$ in real space versus normalized radial distance $\bar{x}$. The asymptotic behavior for small and large $\bar{x}$ (Eq. (8c,d)) are plotted as dashed and dotted lines respectively. (b) Transfer function $\tilde{\phi}(\mathbf{q})$ in the Fourier space versus $q / q_c$.

The real and FT expressions of the transfer function, Equations (7) and (8b) for 2D, are the central new results of our work. A similar treatment yields the transfer function for 1D surfaces where the profile $h(x_1)$ is independent of $x_2$. This transfer function and some applications to 1D surfaces are provided in SI. The remainder of this manuscript studies their applications to a variety of patterned 2D surfaces, as well as characteristics and adhesion of randomly rough surfaces.

## 3. Applications

### 3.1 Flattening of Surfaces with Two-Dimensional Profiles

#### (a) 2D-periodic surface profiles

In many practical situations $h_0(x_1, x_2)$ is a periodic function in 2D. We consider a periodic surface of the form $h_0(x_1, x_2) = A\cos(n\pi x_1 / L_1)\cos(m\pi x_2 / L_2)$ in which $n$ and $m$ are any non-negative integers, $A$ is the amplitude, and $L_1$, $L_2$ are characteristic wavelengths. In the SI, we show that surface stress deforms $h_0(x_1, x_2)$ into

$$h\left(x_1,x_2\right)=\frac{A\cos\left(n\pi x_1/L_1\right)\cos\left(m\pi x_2/L_2\right)}{1+q_c^{-1}\sqrt{\frac{\pi^2n^2}{L_1^2}+\frac{\pi^2m^2}{L_2^2}}}. \tag{9}$$

Similar to the 1D case, surface stress leaves the wavelength unchanged, decreasing instead the amplitude, each *m*, *n* mode by a factor of $1+q_c^{-1}\sqrt{\frac{\pi^2n^2}{L_1^2}+\frac{\pi^2m^2}{L_2^2}}$. (See SI for results on a more generic 2D-periodic surface.) In general, a periodic function $h_0\left(x_1,x_2\right)$ within periods $2L_1$ and $2L_2$ in two directions can be expressed by a 2D Fourier series, that is,

$$\begin{aligned}h_0\left(x_1,x_2\right)=&\sum_{n=0}^{\infty}\sum_{m=0}^{\infty}a_{nm}^0\cos\left(\frac{\pi nx_1}{L_1}\right)\cos\left(\frac{\pi mx_2}{L_2}\right)+\sum_{n=0}^{\infty}\sum_{m=0}^{\infty}b_{nm}^0\cos\left(\frac{\pi nx_1}{L_1}\right)\sin\left(\frac{\pi mx_2}{L_2}\right)\\&+\sum_{n=0}^{\infty}\sum_{m=0}^{\infty}c_{nm}^0\sin\left(\frac{\pi nx_1}{L_1}\right)\cos\left(\frac{\pi mx_2}{L_2}\right)+\sum_{n=0}^{\infty}\sum_{m=0}^{\infty}d_{nm}^0\sin\left(\frac{\pi nx_1}{L_1}\right)\sin\left(\frac{\pi mx_2}{L_2}\right),\end{aligned} \tag{10}$$

The Fourier coefficients $a_{nm}^0,b_{nm}^0,c_{nm}^0,d_{nm}^0$ are defined in the SI. The deformed surface $h\left(x_1,x_2\right)$ is also periodic and is given by (19) except that $\left(a_{nm}^0,b_{nm}^0,c_{nm}^0,d_{nm}^0\right)$ must be replaced by

$$\left(a_{nm},b_{nm},c_{nm},d_{nm}\right)=\frac{\left(a_{nm}^0,b_{nm}^0,c_{nm}^0,d_{nm}^0\right)}{1+q_c^{-1}\sqrt{\frac{\pi^2n^2}{L_1^2}+\frac{\pi^2m^2}{L_2^2}}}. \tag{11}$$

As in the 1D example (see the SI), for large elastocapillary number $\beta\sigma/2GL_1>>1$, the surface profile converges to a limiting profile:

$$\left[h\left(\mathbf{x},\varepsilon>>1\right)-a_{00}\right]\frac{\beta\sigma}{2GL_1}\to\sum_{(n,m)\neq(0,0)}^{\infty}\frac{a_{nm}^0}{\sqrt{\pi^2n^2+\frac{\pi^2m^2L_1^2}{L_2^2}}}\cos\left(\frac{\pi nx_1}{L_1}\right)\cos\left(\frac{\pi mx_2}{L_2}\right), \tag{12}$$

The final shape, when normalized by the elastocapillary number $\beta\sigma/2GL_1$, depends only on the initial geometry. As a specific example, Fig. 3 shows initial and deformed profiles for a periodic structure $h_0\left(x_1,x_2\right)$ in $\left[-L,L\right]\times\left[-L,L\right]$ given by

$$h_0\left(x_1,x_2\right)=\begin{cases}A & x_1\in\left[-L/2,L/2\right],\ x_2\in\left[-L/2,L/2\right]\\0 & \text{otherwise}\end{cases}. \tag{13}$$

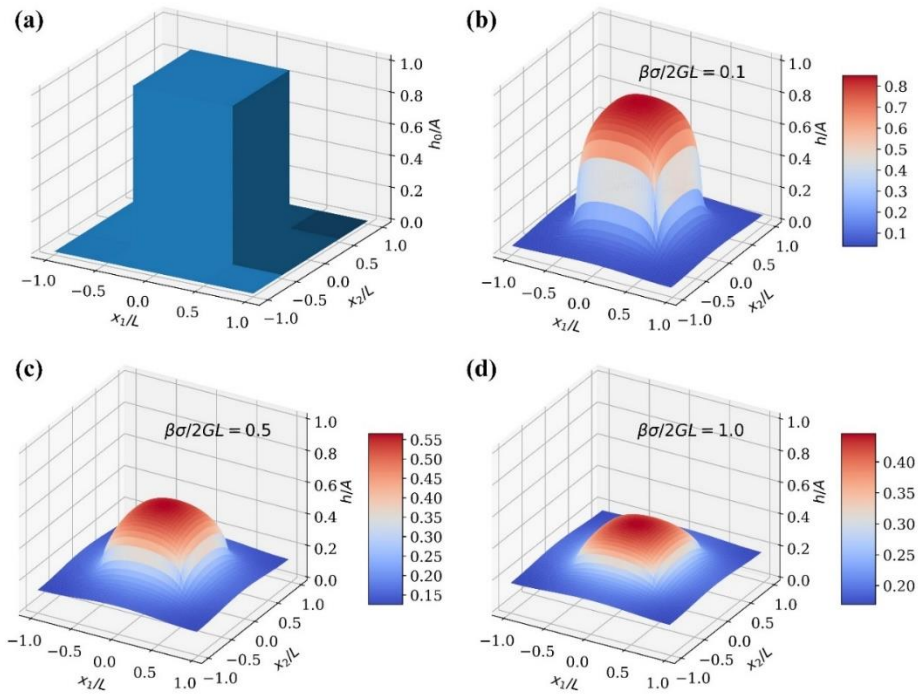


Fig. 3. (a) Initial profile; (b) $\beta\sigma / 2GL = 0.1$; (c) $\beta\sigma / 2GL = 0.5$; (d) $\beta\sigma / 2GL = 1$.

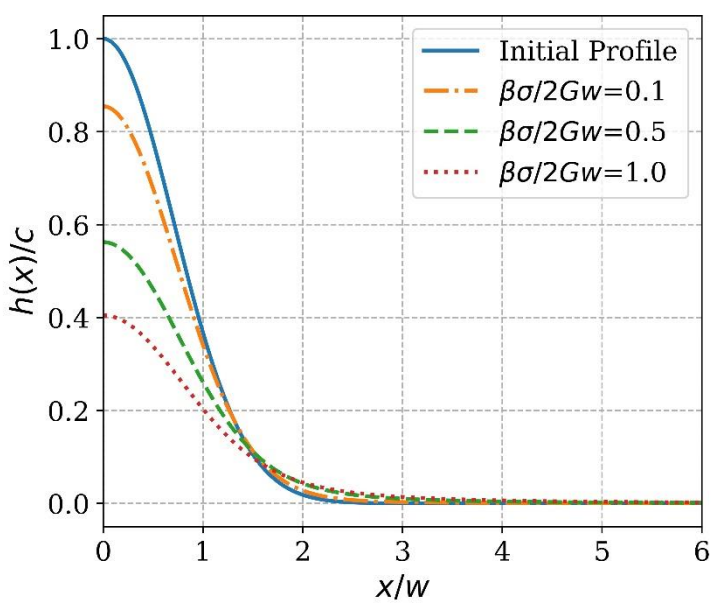


Fig. 4. The deformed shape of a Gaussian bump due to surface stress (dotted lines). The initial shape (without surface stress) is the solid blue line.

**(b) Lifting of a depression or flattening of a bump**

Consider a small depression given by the Gaussian, $h_0\left(x_1, x_2\right) = ce^{-x^2/w^2}$, where $x = \sqrt{x_1^2 + x_2^2}$ (for a bump, $c < 0$); $w$ is its characteristic width. The deformed profile is given by (see the SI)

$$h(x)=\frac{c}{2}\int_0^\infty \frac{\eta e^{-\eta^2/4}}{\left[1+\eta/(q_c w)\right]} J_0\left(\frac{\eta x}{w}\right) d\eta \,. \tag{14}$$

Profiles of $h(x)$ for different elastocapillary number $\beta\sigma/2Gw$ are plotted in Fig. 4.

### 3.2 Flattening and Adhesion of Self-Affine Surfaces

As discussed in the Introduction, surface roughness strongly affects surface properties such as adhesion and friction. The crucial quantity that characterizes roughness is its power spectral density (PSD), $C(\mathbf{q})$; it is the Fourier transform of the autocorrelation function of the surface heights [34,47], and $C(\mathbf{q}) \equiv \left|\tilde{h}(\mathbf{q})\right|^2$. *Self-affine* surfaces [34,48] are an important special case of rough surfaces. They are surfaces with fractal-like topography. They are characterized by a power-law decay of the surface power-spectral density, denoted by $C_0(\mathbf{q})$,

$$C_0(q)=D_0\begin{cases} 0 & q \le q_L \\ q^{-2-2H} & q_L < q < q_s \\ 0 & q \ge q_s \end{cases}, \tag{15}$$

where $q_L$ and $q_s$ are the lower and upper cutoff wave vector respectively. In the following, we define $l_L = 1/q_L$ and $l_s = 1/q_s$. Physically, $l_L$ and $l_s$ correspond to the long and short wavelength cut-offs, respectively. $D_0$ is a constant with dimensions $[L]^{4-2H}$, and $H$ is the Hurst exponent. Typical values of $H$ on scales from atoms to mountains are between 0.7 and 0.9 [49–51]. As noted by [34,49], self-affine scaling can extend over many decades so $q_s >> q_L$. The small scale cut-off is at the molecule scale ($>\sim \mathrm{nm}^{-1}$) while for soft solids a large-scale cut-off is the sample size, or for thin enough samples, flattening due to gravity, i.e., $q_L \approx \sqrt{\rho g/\sigma} \sim \mathrm{mm}^{-1}$. A reasonable value of $q_s/q_L$ is thus $10^6$, which we will use in the remainder of this work. Eq. (15) is a special case in Persson and Gorb [48] of a somewhat more general definition in Jacobs et al. [34], assuming no roll-off.

Jacobs et al. [34] argued that the mechanical response of surfaces is determined by three important statistical measures of the real-space surface topography: the root-mean-square (RMS) height $h_{rms}$, the RMS slope $h'_{rms}$, and the RMS curvature $h''_{rms}$. For isotropic surfaces, the expressions are

$$h_{rms}^2=\frac{1}{2\pi}\int_0^\infty qC(q)\,dq\,,\; h_{rms}'^2=\frac{1}{2\pi}\int_0^\infty q^3C(q)\,dq\,,\; h_{rms}''^2=\frac{1}{8\pi}\int_0^\infty q^5C(q)\,dq\,. \tag{16a-c}$$

For self-affine surfaces, by substituting (15) and (16), and using $q_s >> q_L$, we obtain [34]

$$h_{0rms}^2 = \frac{D_0}{4\pi H} q_L^{-2H} \ , \ h_{0rms}'^2 \approx \frac{D_0}{4\pi(1-H)} q_s^{2-2H} \ , \ h_{0rms}''^2 \approx \frac{D_0}{16\pi(2-H)} q_s^{4-2H} \ . \tag{17a-c}$$

Thus, the RMS height depends on the power at the scale of $q_L$ whereas the RMS slope and curvature are *independent* of $q_L$, meaning that, for a self-affine surface, these latter two characteristics of the surface roughness are determined entirely by the smallest scale surface features. As shown next, these results are dramatically altered by surface stress.

**(a) Effect of surface stress on power-spectral density of self-affine surfaces**

Surface stresses have a dramatic effect on self-affine surfaces at small length scales. In this subsection, we will consider the effect of surface stresses in Fourier space. In the next sub-sections, we'll consider its effect on the statistical measures of the real-space topography. Our result (6) shows that the ratio of the PSD of the final and initial self-affine surfaces is

$$\frac{C(\mathbf{q})}{C_0(\mathbf{q})} = \left|\tilde{h}(\mathbf{q})\right|^2 / \left|\tilde{h}_0(\mathbf{q})\right|^2 = \left[1 + q/q_c\right]^{-2} \tag{18}$$

For soft materials, $q_c$ varies from $10^5\,\mathrm{m}^{-1}$ to $10^8\,\mathrm{m}^{-1}$ as noted in the Introduction. Fig. 5 plots $C(q)$ using $q_L = 10^3\,\mathrm{m}^{-1}$, $q_s = 10^9\,\mathrm{m}^{-1}$ and $H = 0.75$. As shown in Fig. 8, in a log-log plot, the slope of the initial self-affine surface $C_0(q)$ is a constant given by $-2-2H$. When surface stress matters, i.e., when $q_s > q_c > q_L$, $C(q)$ is no longer a straight line in log-log space. Instead, its slope in this plot changes from $-2-2H$ for $q_c > q > q_L$ to $-4-2H$ for $q_s > q > q_c$.

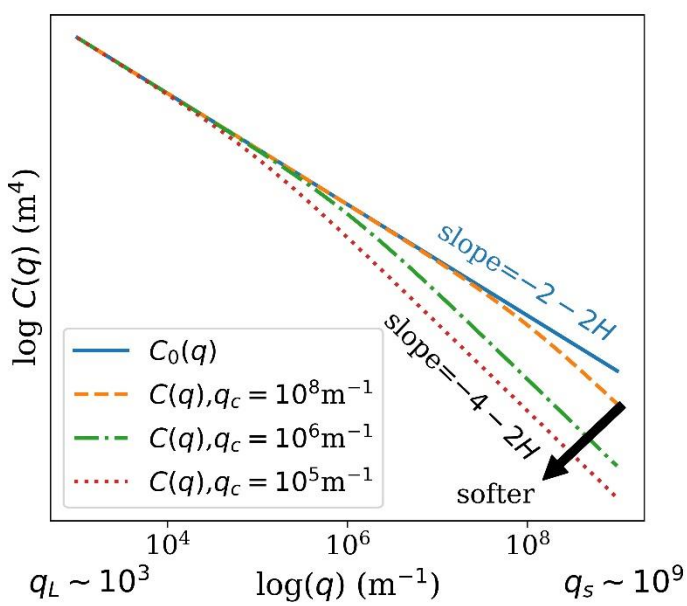

Fig. 5. Log-log plot of $C(q)$ versus $q$ for $H = 0.75$. For $q_s > q_c > q_L$, $C(q) \to C_0(q)$; its slope in this log-log plot is $-2-2H$. In contrast, the slope of $C(q)$ for $q_s > q > q_c$ is $-4-2H = 2-2(H+1) = 2-2H'$ where $H' = H+1$. The figure plots $C(q)$ for three values of $q_c$ from relatively soft (red dotted line) to relatively stiff (orange dashed line).

Thus, the first consequence of deformation driven by surface stress is that the deformed surface is no longer self-affine. (However, because the transfer function is isotropic, isotropy is preserved by surface stress.) More accurately, it is no longer self-affine with a *single* Hurst exponent for $q_L < q < q_s$. Rather, in the soft regime, $q_s > q > q_c$, the surface approximately transformed from one with Hurst exponent $H$ to one with $H$+1. We will often encounter ratios such as $q_c / q_s = l_s / l_c$ and $q_c / q_L = l_L / l_c$. Thus, the ratio of two '$q$'s in Fourier space is the inverse of the ratio of corresponding length scales. In this instance, the ratio $q_c / q_s$ equals the ratio of short cut-off length and the elastocapillary length whereas $q_c / q_L$ represents the ratio of long cut-off length versus the elastocapillary length.

**(b) Effect of surface stress on RMS height**

Consider first the RMS height. Direct integration of (16a) using (15) and (18) gives (see the SI)

$$h_{rms}^2 = \frac{D_0 q_L^{-2H}}{2\pi} \left(q_c / q_L\right)^2 \frac{{}_2F_1\left(2, 2+2H; 3+2H, -q_c / q_L\right)}{\left(2+2H\right)}, \tag{19}$$

where ${}_2F_1$ is the Gauss Hypergeometric function. Similar to the case of no surface stress, *as long as* $q_s / q_L >> 1$, $q_s$ *plays no role in determining the RMS height*. To compare the RMS height with and without surface stress, we form the ratio $h_{rms}^2 / h_{0rms}^2$ using (17a) and (19), i.e.,

$$\frac{h_{rms}^2}{h_{0rms}^2} = \frac{H}{1+H} \left(q_c / q_L\right)^2 {}_2F_1\left(2, 2+2H; 3+2H; -q_c / q_L\right). \tag{20}$$

For $q_L / q_c < 1$, (20) can be expanded in a power series,

$$\frac{h_{rms}^2}{h_{0rms}^2} = \sum_{k=0}^{\infty} \frac{\left(k+1\right)\left(-2H\right)}{-2H+k} \left(-\frac{q_L}{q_c}\right)^k + \frac{H}{1+H} \Gamma\left(3+2H\right) \Gamma\left(-2H\right) \left(\frac{q_L}{q_c}\right)^{2H}. \tag{21}$$

where $\Gamma$ is the Gamma function. Since $H$ typically lies between 0.7 to 0.9, for very hard solids where $q_L / q_c << 1$ equation (21) indicates

$$\frac{h_{rms}^2}{h_{0rms}^2} \approx 1 - \frac{4H}{2H-1}\frac{q_L}{q_c}, \tag{22}$$

A plot of $h_{rms}^2 / h_{0rms}^2$ versus $q_L / q_c$ is shown in Fig. 6(a) using $H = 0.75$. The solution for $H = 0.75$ is exact and is given in the SI. This figure shows surface stress can dramatically reduce the RMS height as the RMS ratio decreases rapidly from 1 as $q_L / q_c$ increases from zero.

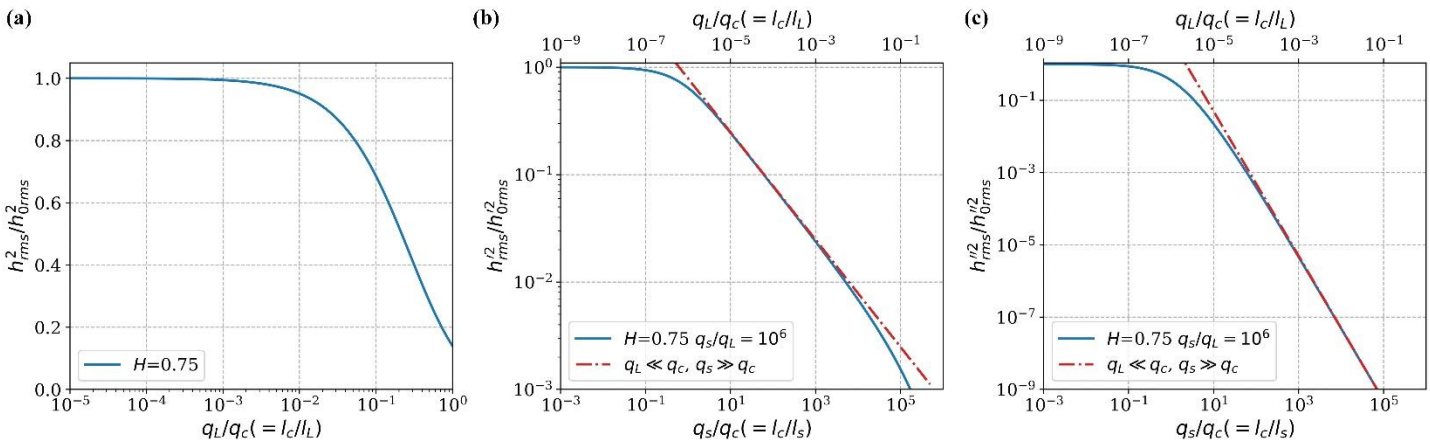


Fig. 6. (a) The ratio of RMS heights is plotted against the elastocapillary number for $H = 0.75$. (b) The ratio of RMS slope is plotted against $q_s / q_c$ for $H = 0.75$ and $q_s / q_L = 10^6$. The red dash-dotted line is (25b). (c) The ratio of RMS curvature is plotted against the elastocapillary number for $H = 0.75$ and $q_s / q_L = 10^6$. Blue solid is the exact solution. The red dash-dot curve is (28b).

**(c) Effect of surface stress on RMS slope**

Next, we consider the RMS slope which, according to Eq. (17b), depends only on the small features, i.e., on $q_s$. Since surface stress tends to smooth preferentially the small-scale features, we expect it to alter this conclusion. The ratio of RMS slopes before and after deformation is (see SI)

$$\frac{h_{rms}'^2}{h_{0rms}'^2} = {}_2F_1\left(2, 2-2H; 3-2H; -q_s/q_c\right) - \left(q_s/q_L\right)^{2H-2} {}_2F_1\left(2, 2-2H; 3-2H; -q_L/q_c\right). \tag{23}$$

Consider first hard solids where $q_s / q_c < 1$. For this case, using the power series expansion for (23) gives

$$\frac{h_{rms}'^2}{h_{0rms}'^2} = \sum_{k=0}^{\infty} \frac{(k+1)(2-2H)}{2-2H+k}\left(-q_s/q_c\right)^k - \left(q_s/q_L\right)^{2H-2} \sum_{k=0}^{\infty} \frac{(k+1)(2-2H)}{2-2H+k}\left(-q_L/q_c\right)^k. \tag{24a}$$

For $0.5 < H < 1$, $q_s >> q_L$, and $q_s / q_c << 1$, then (24a) becomes $h'^2_{rms} = h'^2_{0rms}$. The more general case corresponds to solids soft enough with $q_L / q_c < 1$ but $q_s / q_c > 1$. Using linear transformation formulas and power series expansion for the first term in the right-hand side (RHS) of (23) gives

$$\frac{h'^2_{rms}}{h'^2_{0rms}} = -\frac{(1-H)}{H}\sum_{k=0}^{\infty}\frac{(k+1)(2H)}{(2H+k)}\left[-(q_s/q_c)\right]^{-k-2} + (q_s/q_c)^{-2+2H}\Gamma(3-2H)\Gamma(2H) \\ -(q_s/q_L)^{2H-2}\sum_{k=0}^{\infty}\frac{(k+1)(2-2H)}{2-2H+k}(-q_L/q_c)^k \quad . \tag{25a}$$

For soft solids, $q_L / q_c << 1$ while $q_s / q_c >> 1$ is typical. For this important case, the dominant term in (25a) is

$$\frac{h'^2_{rms}}{h'^2_{0rms}} \approx (q_s/q_c)^{-2+2H}\Gamma(3-2H)\Gamma(2H) \Rightarrow h'^2_{rms} \approx \frac{\Gamma(3-2H)\Gamma(2H)}{4\pi(1-H)} D_0 q_c^{2-2H} . \tag{25b}$$

Eq. (25b) shows that the RMS slope is controlled solely by surface stress through the elastocapillary length. In Fig. 6(b), we plot $h'^2_{rms} / h'^2_{0rms}$ versus $q_s / q_c$ in log-log scale for $q_s / q_L = 10^6$ and $H = 0.75$. The red dash-dotted line is (25b), representing the behavior of soft solids. It is very accurate for $q_s / q_c \geq 10$.

**(d) Effect of surface stress on RMS curvature**

Finally, we consider the RMS curvature. For this case, the ratio of the RMS curvatures is (see SI)

$$\frac{h''^2_{rms}}{h''^2_{0rms}} = {}_2F_1(2, 4-2H; 5-2H; -q_s/q_c) - (q_s/q_L)^{2H-4}\,{}_2F_1(2, 4-2H; 5-2H; -q_L/q_c). \tag{26}$$

Using the same tricks (i.e., linear transformation formulas and power series expansion for hypergeometric functions) and similar arguments in previous subsection, we find, for $q_s / q_c < 1$ (hard solids),

$$\frac{h''^2_{rms}}{h''^2_{0rms}} = \sum_{k=0}^{\infty}\frac{(k+1)(4-2H)}{4-2H+k}(-q_s/q_c)^k - (q_s/q_L)^{2H-4}\sum_{k=0}^{\infty}\frac{(k+1)(4-2H)}{4-2H+k}(-q_L/q_c)^k , \tag{27}$$

In typical situations, $q_s / q_c > 1$ and $q_L / q_c < 1$, we find

$$\frac{h''^2_{rms}}{h''^2_{0rms}} = -(4-2H)\sum_{k=0}^{\infty}\frac{(k+1)}{(2H-2+k)}\left[-(q_s/q_c)\right]^{-k-2} + (q_s/q_c)^{-4+2H}\Gamma(5-2H)\Gamma(2H-2) \\ -(q_s/q_L)^{2H-4}\sum_{k=0}^{\infty}\frac{(k+1)(4-2H)}{4-2H+k}(-q_L/q_c)^k , \tag{28a}$$

The asymptotic behavior for soft solids is obtained from (28), it is

$$\frac{h''^2_{rms}}{h''^2_{0rms}} = \frac{2-H}{1-H}\left(q_s / q_c\right)^{-2}, \qquad q_s / q_c >> 1, q_L / q_c << 1. \tag{28b}$$

In Fig. 6(c), we plot $h''^2_{rms} / h''^2_{0rms}$ versus $q_s / q_c$ in log-log scale for $q_s / q_L = 10^6$ and $H = 0.75$. This plot shows that the RMS curvature ratio drops extremely rapidly from 1 to a small number as $q_s / q_c$ increases from zero. The red dash-dotted line is (28b), representing the behavior of soft solids. It is very accurate for $q_s / q_c > 10$: a condition that is readily satisfied by soft materials.

To summarize the results of this section, the action of surface stress on the characteristics of a rough surface can be profound. If the initial surface roughness is self-affine over the entire range of wave vectors, the deformed surface is no longer so. Instead, if $q_c$ is intermediate in value between $q_s$ and $q_L$ then the surface is approximately self-affine, with the original Hurst exponent $H$ over the low $q$ range and $H+1$ over the high $q$ range. The RMS roughness, slope, and curvature are all attenuated by surface stress. In the case of slope and curvature, for properties typical of soft solids, their dependence on surface properties changes qualitatively. Whereas the RMS slope and curvature of (initially) self-affine surfaces are governed by the small scale wave vector $q_s$, this dependence is replaced by one on $q_c$.

### 3.3 Adhesive contact: effect of surface stress

As discussed previously, surface mechanical properties such as compliance, adhesion, and friction of randomly rough surfaces depend on their PSD. We have just shown how the PSD and its principal characteristics can be profoundly altered by surface stress. This is particularly so at the small length scales, and we now consider how that affects adhesion. We follow the procedure of Persson and Tosatti [42] to study the influence of random surface roughness on the adhesion of elastic structures. In their theory, they consider self-affine surfaces with PSD given by (15). Let us consider the energetics associated with separating a rough surface adhered to a rigid flat plane (per unit area of the flat plane). Start with the elastic body pressed into full contact and adhered to the flat surface. The process of separation increases the energy by $W_o$. In step 2 the flat surface of the elastic body relaxes, releasing elastic energy $U_{el}$. Simultaneously the area increases slightly, thus increasing the surface energy by $\Delta\gamma_a$. This is generally small compared to other terms and will be neglected here. Absent surface stress, the process of separation ends here and the effective work of adhesion is therefore:

$$W_{eff} = W_o + \Delta\gamma_a - U_{el} \approx W_o - U_{el} \tag{29}$$

Within their model, the effective interfacial energy $W_{eff}$ is generally reduced compared to the intrinsic work of adhesion, $W_o$, due to surface roughness. For an infinitely thick plate, they found

$$W_{eff} = W_o \left[ 1 - \frac{2\pi}{\delta_{ad}} \int_0^\infty q^2 C_0^{\text{Persson}}(q) dq \right], \tag{30a}$$

where $\delta_{ad} = 2(1-\nu) W_o / G = \beta W_o / G$ is the adhesive length, and the spectral density denoted by $C_0^{\text{Persson}}(q)$ is

$$C_0^{\text{Persson}}(q) = \frac{4\pi^2}{A_0} \langle \tilde{h}_0^{\text{Persson}}(\mathbf{q}) \tilde{h}_0^{\text{Persson}}(-\mathbf{q}) \rangle, \tag{30b}$$

with $A_0$ the area of the flat interface and

$$\tilde{h}_0^{\text{Persson}}(\mathbf{q}) \equiv \frac{1}{4\pi^2} \iint_D e^{-i(\mathbf{q}\cdot\mathbf{x})} h_0(x_1, x_2) dx_1 dx_2 . \tag{30c}$$

Note in our paper the Fourier transformation (equation (3)) differs from Persson's (equation (30c)) by a factor of $4\pi^2$. We define

$$C_0(q) = \langle \tilde{h}_0(\mathbf{q}) \tilde{h}_0(-\mathbf{q}) \rangle / 4\pi^2 A_0 \tag{31}$$

and it is readily seen that

$$C_0(q) = C_0^{\text{Persson}}(q) \tag{32}$$

Equation (32) allows us to simply replace $C_0^{\text{Persson}}(q)$ with $C_0(q)$ in (30a) to compute the effective work of adhesion. Note in their theory, they did not consider the effect of surface stress so that when the rough surface of the elastic body is removed from the rigid surface, all the elastic energy of surface-flattening is released. This energy is available to contribute to the work required to separate surface or, equivalently to be subtracted from the work of adhesion, which is expressed by (30a). However, in the presence of surface stress only part of this elastic energy is released, since work of flattening the surface is trapped in the elastic body. Let us denote this energy (per unit area) by $W_s$. In the presence of surface stress, we need to add a third step in which the randomly rough surface flattens, increasing energy by $W_s$, and the effective work of adhesion now is

$$W_{eff} = W_o + \Delta\gamma_a - U_{el} + W_s \approx W_o - U_{el} + W_s \tag{33}$$

which is

$$W_{eff} = W_o \left[ 1 - \frac{2\pi}{\delta_{ad}} \int_0^\infty q^2 C_0(q) dq \right] + W_s \tag{34}$$

A schematic showing these three steps is illustrated in the SI.

To obtain explicit expressions for effective work of adhesion, assume first that there is no surface stress so $W_s = 0$, for this case, it can be readily shown that

$$W_{eff} = \begin{cases} W_o\left[1-\dfrac{2\pi D_0}{\delta_{ad}\left(2H-1\right)}\left(q_L^{-2H+1}-q_s^{-2H+1}\right)\right] & H \neq 0.5 \\ W_o\left[1-\dfrac{2\pi D_0}{\delta_{ad}}\ln\left(q_s/q_L\right)\right] & H = 0.5 \end{cases} \tag{35a,b}$$

There is a clear transition when $H = 0.5$. Since for all practical cases $H$ is between 0.7 and 0.9, we consider only $H > 0.5$ so

$$W_{eff} = W_o\left[1-\frac{2\pi D_0 q_L^{-2H+1}}{\delta_{ad}\left(2H-1\right)}\right],\ U_{el} = \frac{2\pi D_0 W_o q_L^{-2H+1}}{\delta_{ad}\left(2H-1\right)} = \frac{2\pi D_0 G q_L^{-2H+1}}{\beta\left(2H-1\right)} \tag{36a,b}$$

where we have used the fact that $q_L / q_s \approx 0$. In this regime where surface stress is neglected, large surface features control adhesion. With non-zero surface stress, we need to compute $W_s$. Since the calculation method is similar to that of Persson and Tosatti [42], we give the details in the SI and state the results here:

$$W_s = \sigma\pi\left(\frac{\beta\sigma}{2G}\right)\int_0^\infty \frac{q^4 C_0\left(q\right)}{\left(1+\dfrac{\beta\sigma}{2G}q\right)^2}dq \tag{37}$$

Using the power spectral density in (15), the integral can be expressed in terms of hypergeometric functions (see the SI); the result is,

$$W_s = \frac{D_0\pi q_S^{3-2H}\sigma}{3-2H}\left(\frac{\beta\sigma}{2G}\right)\left[{}_2F_1\left(2,3-2H;4-2H;-q_s/q_c\right)-\left(q_s/q_L\right)^{2H-3}\,{}_2F_1\left(2,3-2H;4-2H;-q_L/q_c\right)\right] \tag{38}$$

For hard materials, $q_s / q_c < 1$, the second term in (38) can be neglected in comparison with the first, so

$$W_s = \frac{D_0\pi q_S^{3-2H}\sigma}{3-2H}\left(\frac{\beta\sigma}{2G}\right)\sum_{k=0}^{\infty}\frac{\left(k+1\right)\left(3-2H\right)}{4-2H+k}\left[-\left(q_s/q_c\right)\right]^k, \qquad q_s/q_c < 1 \tag{39}$$

The relevant result is the soft solid regime where $q_L / q_c << 1$ and $q_s / q_c >> 1$. By analyzing the behavior of the integral in (37), we show (see SI),

$$W_s \approx \Gamma\left(3-2H\right)\Gamma\left(-1+2H\right)\frac{2\pi D_0 G}{\beta}q_c^{1-2H} \qquad q_L/q_c << 1,\ q_s/q_c >> 1 \tag{40a}$$

Note that in this regime, the elastic energy due to surface stress *is determined solely by the elastocapillary wave number and is independent* of $q_s$ and $q_L$. Note also that the elastic energy $U_{el}$ (see (36b)) has exactly the same form as (40a) except the wavenumber is $q_L$. Specifically, the ratio in this limit is:

$$\frac{W_s}{U_{el}} \approx \Gamma(3-2H)\Gamma(2H)(q_L/q_c)^{2H-1}. \tag{40b}$$

In most soft materials, $q_c$ is between $q_L$ and $q_s$, (40b) shows that surface stress can considerably increase the effective work of adhesion by reducing the amount of energy available to open the interface.

The theory is expected to break down when $W_s \approx U_{el}$ since when it reaches one, the elastic energy associated with surface stress will cancel the elastic energy $U_{el}$; at this point, roughness has no effect on the effective surface adhesion energy. In the mathematical limit where $q_L/q_c \to \infty$, the ratio $W_s/U_{el}$ can be computed using (36b) and (38); it is

$$W_s(q_L/q_c \to \infty)/U_{el} \to 1 \tag{41}$$

We plot $W_s/U_{el}$ versus $q_s/q_c$ for the case of $H = 0.75$ in Fig. 7 using (36b) and (38).

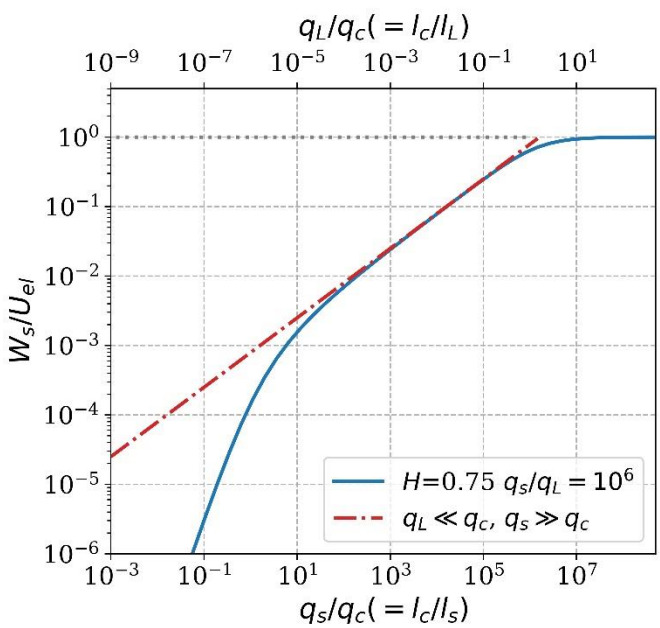


Fig. 7. Ratio of the elastic energy density due to surface tension, $W_s$, and the elastic energy density $U_{el}$ needed to completely flatten the rough surface in the absence of surface stress plotted against $q_s/q_c$ for the case of $H = 0.75$ and $q_s/q_L = 10^6$.

## 4. Summary and Conclusion

In this work we examined in some breadth and depth how in soft materials the surface stress flattens and transforms surface profiles. We first derived basic and general results that relate the initial and deformed (1D and 2D) surface profiles via a transfer function. We obtain explicit forms of the transfer functions that, multiplied by the Fourier transform of the initial profile, yield the Fourier transform of the deformed surface profile. Equivalently, we obtained the form of the real-space transfer function that, in convolution with the real space surface profile, produces the deformed profile. These basic results were applied to study how a number of 1D and 2D surface profiles are transformed by surface stress. We show that 1D and 2D periodic surfaces are flattened but don't change their period. Interestingly, in the limit of large elastocapillary number periodic shapes asymptotically approach a new periodic form that is independent of elastocapillary number. We show that surface stress rounds off sharp features in crack-like defects; this could potentially affect damage and fracture processes in soft materials. Surface stress has a profound effect on self-affine rough surfaces, we found. Specifically, we examined how physically important characteristics of the surface, RMS height, slope, and curvature, are altered as the surface flattens with increasing elastocapillary length. Surface stress preferentially flattens small-scale structures, resulting in a qualitative change in scaling of RMS slope and curvature with roughness parameters and properties. We also examined how the change in surface character affects its adhesion against a rigid flat plane. We show that the energy of flattening subtracts from the elastic energy adhesion penalty usually associated with rough surfaces. For sufficiently compliant surfaces, the roughness penalty can be entirely mitigated. It should be noted that Persson and Tosatti [42] studied the effective work of adhesion for a flat soft solid in contact with a rough rigid surface whereas in our case the soft solid is rough and is in contact with a flat rigid surface. If surface stress is neglected, then the effective work of adhesion for both cases is essentially the same. This is not the case if surface stress is significant. The surface stress of the flat soft surface will resist deformation which decreases the effective work of adhesion. This case is not considered here.

A phenomenon we did not consider here is the thermal fluctuation of surfaces at small scales which can modify the PSD of soft surfaces, as noted by [52–54]. More importantly, we assume that the material is linearly elastic and that the surface stress is isotropic and constant per unit of deformed area. The assumption of linear elasticity is perhaps the most limiting. For example, if a rippled surface of a soft hydrogel is released from its mold, surface stress can squeeze water out and the surface profile will change with time [10,55]. Here we note that immediately after removal from its mold, the gel is incompressible. The gel becomes compressible as solvent squeezes out of the polymer network. Solvent flow will eventually cease as the gel relaxes and reaches equilibrium. The final equilibrium state is elastic and is characterized by the same shear modulus but with a different Poisson's ratio $\nu < 0.5$. Because our material model is elastic, it is unable to capture the transient flow process. Nevertheless, the effect of surface stress can be quantified by the short- and long-time limits where the

hydrogel is elastic since the role of compressibility is specified by $\beta = 2(1-\nu)$. In the short time limit, the gel is incompressible and $\beta = 1$. In the long-time limit, the gel is fully relaxed and $1 < \beta < 2$. Since the elastocapillary length is $\beta\sigma / 2G$, flow increases this length and promotes the flattening effect of surface stress. Soft solids can also exhibit viscoelastic behaviors. Viscoelastic relaxation decreases the shear modulus resulting in increasing elastocapillary length with time. Our analysis for the effect of surface tension on the flattening of structured surface is strictly valid for short or long-time limits. Specifically, for times much shorter (longer) than the characteristic relaxation time, the shear modulus in our model should be replaced with the short (long) time modulus [56]. However, viscoelasticity will significantly change our result on adhesion, since the work to separate two surfaces will be strongly dependent on the history of making contact (compressing the two surfaces together) and separation. We believe that the results presented in this work provide a comprehensive understanding of one of the principal ways in which surface stress acts upon surface profiles. Additionally, the results presented here suggest new experimental work to measure flattened profiles, in particular those of randomly rough surfaces, as well as experiments on how surface properties such as contact compliance, adhesion, and friction are altered by surface stress.

**Ethics:** This work does not involve human subjects or animals.

**Data accessibility:** This work does not have any experimental data. The Jupyter code for numerical results is provided in the electronic supplementary material.

**Authors' contributions:** The problem was conceived in independent discussions between (AJ, NB, RWS, ERD) and (RK, JPG and CYH). CYH formulated and derived the equations and drafted the initial manuscript. Some equations were derived independently by NB with input from AJ, RWS and ERD. ZL carried out all the numerical calculations and rechecked all equations. All authors participated in the writing of the manuscript. All authors gave final approval for publication and agree to be held accountable for the work performed therein.

**Competing interests:** We do not have competing interests.

**Funding:** CYH is supported by National Science Foundation, USA MoMS program under grant number 1903308. JPG thanks the financial support from Japan Society for the Promotion of Science (JSPS) KAKENHI (grant no. JP17H06144).

**Acknowledgements:** CYH acknowledges Soft Matter GI-CoRE of Hokkaido University who supported his visit. We are grateful to the reviewers for their helpful comments.

**References**

1. Style RW, Jagota A, Hui C-Y, Dufresne ER. 2017 Elastocapillarity: Surface Tension and the Mechanics of Soft Solids. *Annual Review of Condensed Matter Physics* **8**, 99–118. (doi:10.1146/annurev-conmatphys-031016-025326)
2. Rowlinson JS, Widom B. 2013 *Molecular theory of capillarity*. Courier Corporation.
3. Gennes P-G de, Brochard-Wyart F, Quéré D. 2010 *Capillarity and wetting phenomena: drops, bubbles, pearls, waves*. New York, NY: Springer.
4. Butt H-J, Graf K, Kappl M. 2003 *Physics and chemistry of interfaces*. Weinheim: Wiley-VCH.
5. Dalvi S, Gujrati A, Khanal SR, Pastewka L, Dhinojwala A, Jacobs TDB. 2019 Linking energy loss in soft adhesion to surface roughness. *Proc Natl Acad Sci USA* **116**, 25484–25490. (doi:10.1073/pnas.1913126116)
6. Mora S, Phou T, Fromental J-M, Pismen LM, Pomeau Y. 2010 Capillarity Driven Instability of a Soft Solid. *Phys. Rev. Lett.* **105**, 214301. (doi:10.1103/PhysRevLett.105.214301)
7. Mora S, Maurini C, Phou T, Fromental J-M, Audoly B, Pomeau Y. 2013 Solid Drops: Large Capillary Deformations of Immersed Elastic Rods. *Phys. Rev. Lett.* **111**, 114301. (doi:10.1103/PhysRevLett.111.114301)
8. Paretkar D, Xu X, Hui C-Y, Jagota A. 2014 Flattening of a patterned compliant solid by surface stress. *Soft Matter* **10**, 4084–4090. (doi:10.1039/C3SM52891J)
9. Hui CY, Jagota A, Lin YY, Kramer EJ. 2002 Constraints on Microcontact Printing Imposed by Stamp Deformation. *Langmuir* **18**, 1394–1407. (doi:10.1021/la0113567)
10. Berman JD, Randeria M, Style RW, Xu Q, Nichols JR, Duncan AJ, Loewenberg M, Dufresne ER, Jensen KE. 2019 Singular dynamics in the failure of soft adhesive contacts. *Soft Matter* **15**, 1327–1334. (doi:10.1039/C8SM02075B)
11. Liu Z, Bouklas N, Hui C-Y. 2020 Coupled flow and deformation fields due to a line load on a poroelastic half space: effect of surface stress and surface bending. *Proc. R. Soc. A* **476**, 20190761. (doi:10.1098/rspa.2019.0761)
12. Carrillo J-MY, Dobrynin AV. 2012 Contact Mechanics of Nanoparticles. *Langmuir* **28**, 10881–10890. (doi:10.1021/la301657c)
13. Hui C-Y, Liu T, Salez T, Raphael E, Jagota A. 2015 Indentation of a rigid sphere into an elastic substrate with surface tension and adhesion. *Proceedings of the Royal Society A: Mathematical, Physical and Engineering Sciences* **471**, 20140727–20140727. (doi:10.1098/rspa.2014.0727)
14. Salez T, Benzaquen M, Raphaël É. 2013 From adhesion to wetting of a soft particle. *Soft Matter* **9**, 10699. (doi:10.1039/c3sm51780b)
15. Style RW, Hyland C, Boltyanskiy R, Wettlaufer JS, Dufresne ER. 2013 Surface tension and contact with soft elastic solids. *Nature Communications* **4**, 2728.
16. Xu X, Jagota A, Hui C-Y. 2014 Effects of surface tension on the adhesive contact of a rigid sphere to a compliant substrate. *Soft Matter* **10**, 4625–4632. (doi:10.1039/C4SM00216D)
17. Liu Z, Jensen KE, Xu Q, Style RW, Dufresne ER, Jagota A, Hui C-Y. 2019 Effects of strain-dependent surface stress on the adhesive contact of a rigid sphere to a compliant substrate. *Soft Matter* **15**, 2223–2231. (doi:10.1039/C8SM02579G)
18. Cao Z, Dobrynin AV. 2015 Polymeric Droplets on Soft Surfaces: From Neumann's Triangle to Young's Law. *Macromolecules* **48**, 443–451. (doi:10.1021/ma501672p)
19. Hui C-Y, Jagota A. 2015 Planar equilibrium shapes of a liquid drop on a membrane. *Soft Matter* **11**, 8960–8967. (doi:10.1039/C5SM02157J)
20. Jerison ER, Xu Y, Wilen LA, Dufresne ER. 2011 Deformation of an Elastic Substrate by a Three-Phase Contact Line. *Phys. Rev. Lett.* **106**, 186103. (doi:10.1103/PhysRevLett.106.186103)
21. Marchand A, Das S, Snoeijer JH, Andreotti B. 2012 Contact Angles on a Soft Solid: From Young's Law to Neumann's Law. *Physical Review Letters* **109**, 236101. (doi:10.1103/PhysRevLett.109.236101)
22. Liu T, Liu Z, Jagota A, Hui C-Y. 2020 Droplets on an elastic membrane: Configurational energy balance and modified Young equation. *Journal of the Mechanics and Physics of Solids* **138**, 103902. (doi:10.1016/j.jmps.2020.103902)

23. Style RW, Boltyanskiy R, Che Y, Wettlaufer JS, Wilen LA, Dufresne ER. 2013 Universal Deformation of Soft Substrates Near a Contact Line and the Direct Measurement of Solid Surface Stresses. *Phys. Rev. Lett.* **110**, 066103. (doi:10.1103/PhysRevLett.110.066103)
24. Wu H, Liu Z, Jagota A, Hui C-Y. 2018 Effect of large deformation and surface stiffening on the transmission of a line load on a neo-Hookean half space. *Soft Matter* **14**, 1847–1855. (doi:10.1039/C7SM02394D)
25. Andreotti B, Snoeijer JH. 2020 Statics and Dynamics of Soft Wetting. *Annu. Rev. Fluid Mech.* **52**, 285–308. (doi:10.1146/annurev-fluid-010719-060147)
26. Limat L. 2012 Straight contact lines on a soft, incompressible solid. *The European Physical Journal E* **35**, 134. (doi:10.1140/epje/i2012-12134-6)
27. Dervaux J, Limat L. 2015 Contact lines on soft solids with uniform surface tension: analytical solutions and double transition for increasing deformability. *Proceedings of the Royal Society A: Mathematical, Physical and Engineering Sciences* **471**, 20140813. (doi:10.1098/rspa.2014.0813)
28. Snoeijer JH, Rolley E, Andreotti B. 2018 Paradox of Contact Angle Selection on Stretched Soft Solids. *Phys. Rev. Lett.* **121**, 068003. (doi:10.1103/PhysRevLett.121.068003)
29. Olives J. 2010 Surface thermodynamics, surface stress, equations at surfaces and triple lines for deformable bodies. *J. Phys.: Condens. Matter* **22**, 085005. (doi:10.1088/0953-8984/22/8/085005)
30. Cheng Z *et al.* 2020 The surface stress of biomedical silicones is a stimulant of cellular response. *Sci Adv* **6**, eaay0076. (doi:10.1126/sciadv.aay0076)
31. Jagota A, Paretkar D, Ghatak A. 2012 Surface-tension-induced flattening of a nearly plane elastic solid. *Phys. Rev. E* **85**, 051602. (doi:10.1103/PhysRevE.85.051602)
32. Lapinski N, Liu Z, Yang S, Hui C-Y, Jagota A. 2019 A surface with stress, extensional elasticity, and bending stiffness. *Soft Matter* **15**, 3817–3827. (doi:10.1039/C9SM00075E)
33. Mullins WW. 1959 Flattening of a Nearly Plane Solid Surface due to Capillarity. *Journal of Applied Physics* **30**, 77–83. (doi:10.1063/1.1734979)
34. Jacobs TDB, Junge T, Pastewka L. 2017 Quantitative characterization of surface topography using spectral analysis. *Surf. Topogr.: Metrol. Prop.* **5**, 013001. (doi:10.1088/2051-672X/aa51f8)
35. Fuller KNG, Tabor D. 1975 The effect of surface roughness on the adhesion of elastic solids. *Proceedings of the Royal Society of London. A. Mathematical and Physical Sciences* **345**, 327–342. (doi:10.1098/rspa.1975.0138)
36. Pastewka L, Robbins MO. 2014 Contact between rough surfaces and a criterion for macroscopic adhesion. *Proc Natl Acad Sci USA* **111**, 3298. (doi:10.1073/pnas.1320846111)
37. Persson BNJ, Albohr O, Tartaglino U, Volokitin AI, Tosatti E. 2004 On the nature of surface roughness with application to contact mechanics, sealing, rubber friction and adhesion. *Journal of Physics: Condensed Matter* **17**, R1–R62. (doi:10.1088/0953-8984/17/1/r01)
38. Kendall K. 2007 *Molecular adhesion and its applications: the sticky universe*. Springer Science & Business Media.
39. Greenwood JA, Williamson JBP, Bowden FP. 1966 Contact of nominally flat surfaces. *Proceedings of the Royal Society of London. Series A. Mathematical and Physical Sciences* **295**, 300–319. (doi:10.1098/rspa.1966.0242)
40. Maugis D. 1996 On the contact and adhesion of rough surfaces. *Journal of Adhesion Science and Technology* **10**, 161–175. (doi:10.1163/156856196X00832)
41. Persson BNJ. 2008 On the elastic energy and stress correlation in the contact between elastic solids with randomly rough surfaces. *Journal of Physics: Condensed Matter* **20**, 312001. (doi:10.1088/0953-8984/20/31/312001)
42. Persson BNJ, Tosatti E. 2001 The effect of surface roughness on the adhesion of elastic solids. *J. Chem. Phys.* **115**, 5597–5610. (doi:10.1063/1.1398300)
43. Persson BNJ. 2002 Adhesion between Elastic Bodies with Randomly Rough Surfaces. *Phys. Rev. Lett.* **89**, 245502. (doi:10.1103/PhysRevLett.89.245502)

44. Guduru PR. 2007 Detachment of a rigid solid from an elastic wavy surface: Theory. *Journal of the Mechanics and Physics of Solids* **55**, 445–472. (doi:10.1016/j.jmps.2006.09.004)
45. Guduru PR, Bull C. 2007 Detachment of a rigid solid from an elastic wavy surface: Experiments. *Journal of the Mechanics and Physics of Solids* **55**, 473–488. (doi:10.1016/j.jmps.2006.09.007)
46. Vajpayee S, Khare K, Yang S, Hui C-Y, Jagota A. 2011 Adhesion selectivity using rippled surfaces. *Advanced Functional Materials* **21**, 547–555.
47. Duparré A, Ferre-Borrull J, Gliech S, Notni G, Steinert J, Bennett JM. 2002 Surface characterization techniques for determining the root-mean-square roughness and power spectral densities of optical components. *Appl. Opt.* **41**, 154. (doi:10.1364/AO.41.000154)
48. Persson BNJ, Gorb S. 2003 The effect of surface roughness on the adhesion of elastic plates with application to biological systems. *The Journal of Chemical Physics* **119**, 11437–11444. (doi:10.1063/1.1621854)
49. Gagnon J-S, Lovejoy S, Schertzer D. 2003 Multifractal surfaces and terrestrial topography. *Europhysics Letters (EPL)* **62**, 801–807. (doi:10.1209/epl/i2003-00443-7)
50. Gagnon J-S, Lovejoy S, Schertzer D. 2006 Multifractal earth topography. *Nonlinear Processes in Geophysics* **13**, 541–570. (doi:10.5194/npg-13-541-2006)
51. Mandelbrot BB, Passoja DannE, Paullay AJ. 1984 Fractal character of fracture surfaces of metals. *Nature* **308**, 721–722. (doi:10.1038/308721a0)
52. Mecke KR, Dietrich S. 1999 Effective Hamiltonian for liquid-vapor interfaces. *Phys. Rev. E* **59**, 6766–6784. (doi:10.1103/PhysRevE.59.6766)
53. Buzza DMA. 2002 General Theory for Capillary Waves and Surface Light Scattering. *Langmuir* **18**, 8418–8435. (doi:10.1021/la011713d)
54. Seydel T, Tolan M, Ocko BM, Seeck OH, Weber R, DiMasi E, Press W. 2002 Freezing of capillary waves at the glass transition. *Phys. Rev. B* **65**, 184207. (doi:10.1103/PhysRevB.65.184207)
55. Ang I, Liu Z, Kim J, Hui C-Y, Bouklas N. 2020 Effect of elastocapillarity on the swelling kinetics of hydrogels. *Journal of the Mechanics and Physics of Solids* **145**, 104132. (doi:10.1016/j.jmps.2020.104132)
56. Hui C-Y, Jagota A. 2016 Effect of surface tension on the relaxation of a viscoelastic half-space perturbed by a point load. *Journal of Polymer Science Part B: Polymer Physics* **54**, 274–280. (doi:10.1002/polb.23920)